RSC Advances

Electroless Nickel Coated Nano-Clay for Electrolytic Removal of Hg (II) Ions

Journal:	*RSC Advances*
Manuscript ID:	RA-ART-07-2014-006988.R2
Article Type:	Paper
Date Submitted by the Author:	10-Sep-2014
Complete List of Authors:	Arora, Rajat; Indian Institute Of Technology (BHU), Department of Metallurgical Engineering Singh, Nitesh; Defence Institute of Advanced Technology, Materials Engineering KANDASUBRAMANIAN, BALASUBRAMANIAN; Defence Institutue Of Advanced Technology, Materials Engineering Alegaonkar, Prashant; Defence Institutue Of Advanced Technology, cDepartment of Applied Physics

Cite this: DOI: 10.1039/c0xx00000x

www.rsc.org/xxxxxx

ARTICLE TYPE

Electroless Nickel Coated Nano-Clay for Electrolytic Removal of Hg (II) Ions

Rajat Arora[a], Nitesh Singh[b], Balasubramanian K.[b]* Prashant Alegaonkar[c]

Received (in XXX, XXX) Xth XXXXXXXXX 20XX, Accepted Xth XXXXXXXXX 20XX
DOI: 10.1039/b000000x

Footprint existence and accumulation of cataclysmic Hg(II) ions in aqueous media poses severe threat to biological ecosystem and necessitate immediate measures for its regulation. In this context, we have elucidated electrolytic removal of Hg (II) ions from prepared solution, akin to effluent system, utilizing novel electroless nickel coated nanoclay electrodes. The dependence of adsorption efficiency on several parameters including initial pH (pH= 3 to 8), initial metal ion concentration (25-100mg/L), amount of nickel coated on nanoclay has been studied. Optimized removal percentage of 70% was recorded at pH 6, when distance between the electrodes was 4cm and a current density ranging from 2-2.5 A dm^{-2} was passed for duration of 60 minutes. No considerable differences in removal efficiency were registered with varying initial metal ion concentration (25-100mg/L). Moreover, the removal efficiency was observed to be high at slightly acidic pH (pH = 6), however, in highly acidic solution (pH = 3-4), low adsorption efficiency was recorded due to electrostatic repulsion caused by H^+ ions. Nickel coating over nanoclay of volume % 15 or greater was found to exhibit optimised conductivity. SEM and FESEM analysis affirmed the uniform deposition of nickel over nano clay. The uptake of Hg (II) ions predominantly followed pseudo second-order kinetics, validated by high values of regression coefficient at all concentrations and Freundlich equilibrium isotherm model was better to predict equilibrium adsorption based on linearized correlation coefficient (R^2 =0.99).

1. Introduction

Discharge of heavy metals as untreated effluents in aqueous media through industrial and other anthropogenic channels is of paramount consideration from both environmental and biological perspectives[1-2]. Mercury and its derivatives enters the environment primarily through improper discharge of industrial (metal, pulp, paper, and chlor-alkali) effluents, burning of fossil fuels, pharmaceutical and cosmetic preparations, accumulation in fishes, thermometers and fluorescent light manufacturing units[3-4]. Being a well known cataclysmic heavy metal, with exceptionally high toxicity, it has brought out several massive calamities, for instance, in Japan (1956), mercury contamination decimated more than 200 lives through ingestion of fish incorporating fatal mercury[5]. This further explains the bioaccumulation of mercury and other heavy metals in food chains and interrelation of human and their environment. Mercury being a naturally known carcinogenic, mutagenic and teratogenic can cause gastrointestinal damage, skin cancers, bladder and kidney cancer, cardio-vascular, neurological and endocrine disorders in the human body[6]. Elevated concentration of mercury is firmly associated with deterioration of pulmonary and kidney functions. Furthermore, numbness of the lips and limbs are the primary and introductory symptoms of mercury poisoning. Excessive levels of contamination can successively lead to permanent breakdown of the nervous system[7].

According to USEPA, permitted mercury content is 2µg/L[8], whereas the World Health Organisation (WHO) and China have recommended an extremum of 1.0µg L^{-1} inorganic mercury content in drinking water[9]. The accepted discharge limit of wastewater for total mercury is 10.0µg/L[10]. Various contemporary techniques such as chemical precipitation[11], membrane filtration[12], ion exchange[13], photo reduction[14], adsorption[15], chelate precipitation[16] have been explored for reducing the mercury content from waste water with a collective aim to cutback precarious effects of mercury and its derivatives, among which adsorption has been widely exploited and put to use[17]. Applicability of other techniques has been limited for small scale operations, whereas, sludge deposition, technical and/or economic constraints ascribes to their restricted pertinence and obsoleteness at large scale[18]. Also, various kinds of bio sorbents including sheep and camel bone charcoal[19-21] have been explored for effective elimination of mercury from wastewater. Iron and aluminium electrodes by electrocoagulation[18], magnetized cellulose porous beads [22], p (GMA-MMA-EGDMA) magnetic beads[6] have also been tested for Hg (II) ions removal from aqueous system. Moreover, electrochemical method for eradication of metal ions from industrial effluents has gained immense significance in recent past due to facile restoration of metal without any subsequent treatment of the obtained metal[23]. Cathodes with ternary dimensions have also been considered and put into effect on account of their larger specific surface area and accelerated mass transfer rates[24].

Considering the existing literatures, the present work focuses at electrolytic elimination of Hg(II) ions from mimicked aqueous system exploiting a novel material, electroless nickel coated nano

clay, which has not been yet reported and used. The electroless nickel coated nanoclay electrodes were prepared through a series of steps viz. sensitisation, activation and nickel coating, using the untreated nanoclay. Further, a series of batch sorption experiments were conducted electrolytically with varying pH, initial metal ion concentration and chloride concentration, optimized conditions being pH 6, distance between the electrodes 4cm, and duration 60 minutes, with no significant effect of initial metal ion concentration on adsorption efficiency. The prepared sorbent could retain 70% of the Hg (II) ions at optimized conditions. The sorption kinetics was examined to predict the pathway of the experiment, using pseudo first-order, pseudo second order and intra-particle diffusion kinetic models. Moreover, the equilibrium adsorption conditions were inspected using the Langmuir and Freundlich isotherm models to estimate maximum uptake capacity of an adsorbent. This technique offers improved selectivity, low operating costs and effective removal of Hg (II) ions from aqueous media to prescribed limits and guidelines.

2. Materials and Methods

2.1 Materials

Macuplex^{R} Activator D-34C; a liquid catalyst system which incorporates sensitizer and activator in a unit system, was utilized for pre-treatment of specimen before electroless nickel coating and ELNIC 204; a stable electroless nickel solution was purchased from UK for electroless nickel plating[25]. Mercury Chloride ($HgCl_2$ with >99.5% assay), Hydrochloric Acid (HCl with 99% purity), Sodium Hydroxide (NaOH with 98% purity), Potassium Iodide (KI with >99.5% assay) and Rhodamine B (Lobachemie with > 99% assay) were acquired from Merck Inc. India. Unmodified nano clay was supplied from Southern Clay, USA. All the chemicals and reagents were of analytical grade and used as received without any further treatment, unless mentioned otherwise. Deionized water was utilized for all the experimental purposes, which was procured from Millipore Milli-Q system.

2.2 Fabrication of Electroless nickel coated nano clay

The electroless coating technique as illustrated by B. Kandasubramanian[25] was implemented to execute the uniform accumulation of electroless nickel over nanoclay. Briefly, the ELNIC 204 solution consists of two process components, first, ELNIC 204A which is the nickel component and ELNIC 204B act as a reducer and the complexing constituent. This process was employed to deposit an ultra bright, low-medium phosphorus content coating on a variety of substrates. The process consisted of 3 steps:

Step 1: Sensitisation- Pre-treatment of surface with stannous chloride – to sensitize the surface of nano clay with Sn^{2+} ions.

Step 2: Activation – following the initial step, it was treated with 2% solution of palladium chloride ($PdCl_2$). The Pd^{2+} ions were reduced to Pd, which acted as the catalytic site for electroless nickel coating.

$$Pd^{2+} + Sn^{2+} \longrightarrow Pd^{0} + Sn^{4+}$$

Step 3: Nickel coating - the pre-treated nano clay was treated with the nickel solution at pH 5 in the temperature range of 85-90 °C.

Three dimensional electrodes were fabricated using nickel coated nano clay; the electrode dimensions were 10 × 10 × 2 mm.

2.3 Characterization:

The morphology and particle size of the nickel coated nanoclay were analyzed using (FESEM) Field emission scanning electron microscopy (Carl-Zeiss, Germany). The samples were sputtered using Au-Pd for 75 seconds in 10 mA under the pressure of 0.6 x 10^{-2} Pa and were tested in the microscope at 5kV and the images were obtained under 15 KX and 50 KX, magnification. Energy dispersive X-ray (EDX) spectroscopy was used to evaluate chemical composition and elemental analysis with the system resolution of 127eV. Fourier Transform infrared (FT-IR) spectrophotometer was carried out for functional group analysis (Bruker-380, USA) in the wavelength range of 400-4000 cm^{-1}. Different samples of Nickel coated nanoclay were analysed by X-ray diffraction (XRD) using Bruker AXS D8 advance diffractometer, USA with Cu Kα radiation. Atomic Force Microscopy (AFM) was used to evaluate the surface roughness (Asylum research, an oxford instrument company, UK) in tapping mode. Raman spectra's were recorded using the Renishaw in micro- Raman spectrometer using argon laser excitation wavelength of 632.81nm at 20Mw power with illumination spot size of 1μm and acquisition time 90sec.

2.4 Experimental setup

Batch experiments for Hg(II) decontamination were conducted using the specially designed electrodes at room conditions. The electrolysis bath consisted of a glass beaker (250 mL capacity) with a PVC cap attached to it. The two electrodes were kept immersed into the solution through this lid and the experiments were performed under vigorous and continuous magnetic stirring for 60 minutes. Fig.11 illustrates the schematic of the experimental arrangement. DC power source was adopted to impart current density in the range of 2.0-2.5 A dm^{-2}. The electrodes were connected to the power source through copper coils. The electrodes were fabricated in such a manner that they can avoid any possible contact between the Hg(II) solution and copper coils. The electrodes were immersed in 100 mL Hg(II) solution of varying concentrations, (25-100 mg/L) while maintaining a distance of 4cm between them. The diminishing Hg(II) concentration was periodically monitored, using Rhodamine B[26] as the complexing agent and the absorbance was recorded using Nanodrop UV-Visible Spectrophotometer (NANO DROP, ND-1000).

Mercury removal was quantized in terms of adsorption capacity (q_e) and adsorption efficiency (E) as[27]:

$$q_e = ((C_o - C_e)/w] \text{ X } V \quad (1)$$

$$E = [(C_o - C_e)/C_o] \text{ X } 100 \quad (2)$$

C_o and C_e are the initial and equilibrium metal ion concentration (mg L^{-1}) respectively. V is the volume of the solution (L) and w is the amount of sorbent used (g).

3. Results and Discussion

The electrolytic sorption experiments were performed using electroless nickel coated nanoclay under optimised conditions. Furthermore, conductivity of the coated nano clay was scrutinized by recording volume resistivity with varying the percentage of nickel coated on nanoclay. A continuous decrease in the volume resistivity was registered with increment in volume percent of nickel (Fig. 1). Nickel coating of more than 15 volume % exhibited effective conductivity and thereafter, all experiments were conducted utilizing electrodes bearing 16 volume % of nickel coating.

The current density was fixed in the range 2.0 - 2.5 A dm^{-2} for optimal removal. 70% removal efficiency was observed at current density of 2.0 -2.5 A dm^{-2} at 30 °C. Besides, it was observed that current density inferior to the optimised range (<2.0 A dm^{-2}) was ineffective and presented unsatisfactory results. Nevertheless, with application of higher current density, the duration of experiment was curtailed while maintaining the same removal efficiency.

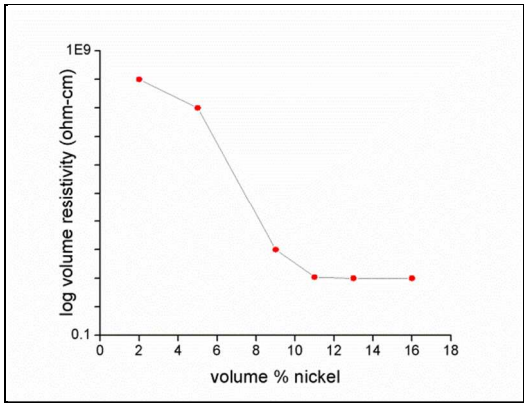

Fig. 1: Variation of Conductivity of electroless nickel coated nano clay with volume % nickel

3.1 Characterization of Unmodified nano-clay and Nickel coated nano-clay

3.1.1 Scanning electron micrographs

The uniform nickel coating on the nano-clay was confirmed from the microscopic analysis. Fig. 2a shows the FESEM micrograph of the pristine nano-clay which illustrates the formation of plate like structure without any porosity or the formation of globular structure[19]. Fig. 2b and 2c are the SEM and FESEM micrographs of electroless nickel coated nano-clay, which clearly depicts the formation of porous globules in the range of 300-400nm due to extensive coverage of uniform electroless nickel over the clay surface using the ELNIC system. Also, processing parameters like aspect ratio, agitation, concentration of Ni influenced the formation of globule like structure as shown in Fig. 2(c) due to folding of nano-clay platelets.

The specific surface area and porosity may play an important role in adsorption process, was further confirmed by BET analysis. The specific surface area of nickel coated nanoclay was obtained as high as 54.38m^2/g as compared to nanoclay which was 30.33m^2/g[28]. The porous structure enhanced the adsorption process based on obtained average pore size and pore volume of nickel coated nano-clay, which were 66.42 nm and 0.204 cm^3/g. Therefore, it rapidly diffused the Hg(II) ions into the internal pores of the adsorbent for contact with the adsorptive sites.

The elemental composition was characterized using energy dispersive analysis (Fig.3) which confirms the granular deposition of nickel on the coated nanoclay and the formation of oxides near the edges of the electrode surface at high current density[25]. The ingredients of nanoclay have been explored and are found to be comprised of potassium, aluminium, silica, and magnesium[56].

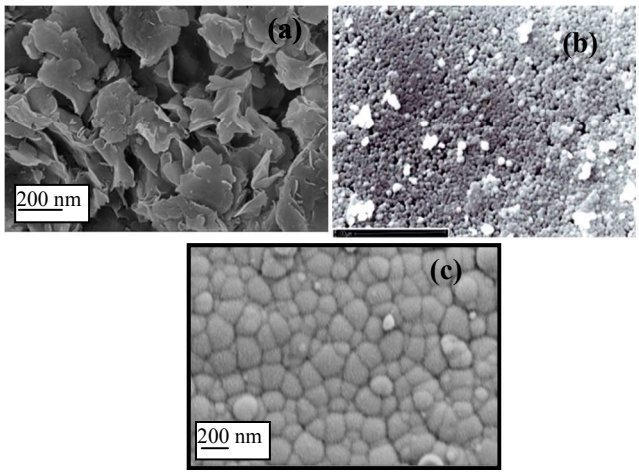

Fig. 2: (a) FESEM image of pristine nano-clay (b) SEM image of nickel coated nano-clay (c) FESEM image of nickel coated nano-clay

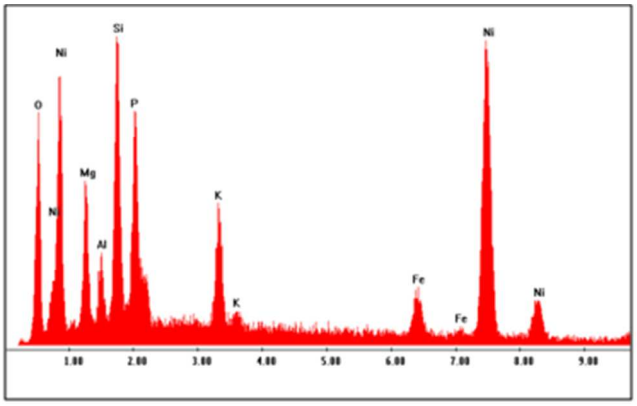

Fig.3: EDX spectrum of electroless nickel coated nanoclay through elemental analysis

3.1.2 Compositional Analysis by FT-IR

The FT-IR spectra of unmodified nanoclay and nickel coated nanoclay are displayed in Figure 4. The unmodified nanoclay mainly contains the Si-O (Si) asymmetric stretching bands (1085cm^{-1}), asymmetric vibration of Si-O (H) is near 975cm^{-1}, O-H stretching bands as a small peaks (3594 and 3735cm^{-1})[29]. However, the intense peaks with maximum have been observed at 529 and 1113cm^{-1} for Si-O bending vibration and Si-O out-of-plane stretching vibration in nickel coated nanoclay which was confirmed by Prog *et al*[30]. After modification with nickel coating, the new intense peaks at 3634 and 3735cm^{-1} corresponds to the –OH group that is bonded to aluminium and magnesium in clay[31]. New peaks at 1557cm^{-1} with a small shoulder at 1457cm^{-1} corresponds to $–NH_2$ vibration. The appearance of these new peaks suggested the coating of nickel over the -OH and -NH groups on the broken edges of the silicate layers, to form Ni-O complexes which may increase the adsorption capacity of heavy metal ions[32].

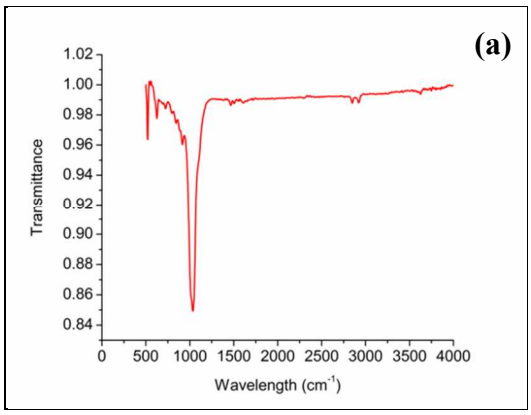

Fig. 4: FT-IR spectra of (a) Unmodified Nanoclay (b) Nickel coated nano-clay

3.1.3 X- Ray Diffraction Pattern Analysis

The XRD Pattern of unmodified nanoclay, nickel coated nanoclay and Hg (II) - nickel coated nanoclay was represented in Fig. 5. The XRD pattern of nanoclay powder investigated the shift to lower 2θ values of the (001) and (002) reflections due to swelling in inter lamellar of the clay mineral space[33]. The XRD peaks as in figure 5(b) shows that the electroless nickel crystallised to a two-phase mixture of nickel and Ni_3P. The characteristic peak for nickel appears at 45.49^0 (111) and 53.041^0 (200) indicates the presence of nickel over clay gallaries[34]. Additional Peaks appears at 26.2^0 and 76.3^0 are of nickel phosphide. The shoulder peak existing right to nickel 52.6^0(111) peak is the peak of Ni_3P reflecting the existence of a different phase, which affects the crystal structure of nickel in the system[35]. XRD pattern of Hg-nickel coated nanoclay as shown in Fig. 5(c) attributes the appearance of broad peak near 25- 35^0 represents the exfoliation and dispersion of nanoclay with electroless nickel to form an integrity type matrix. Also, a broad peak appears around 45^0 depicts the adsorption of Hg(II) onto the nickel coated nanoclay.

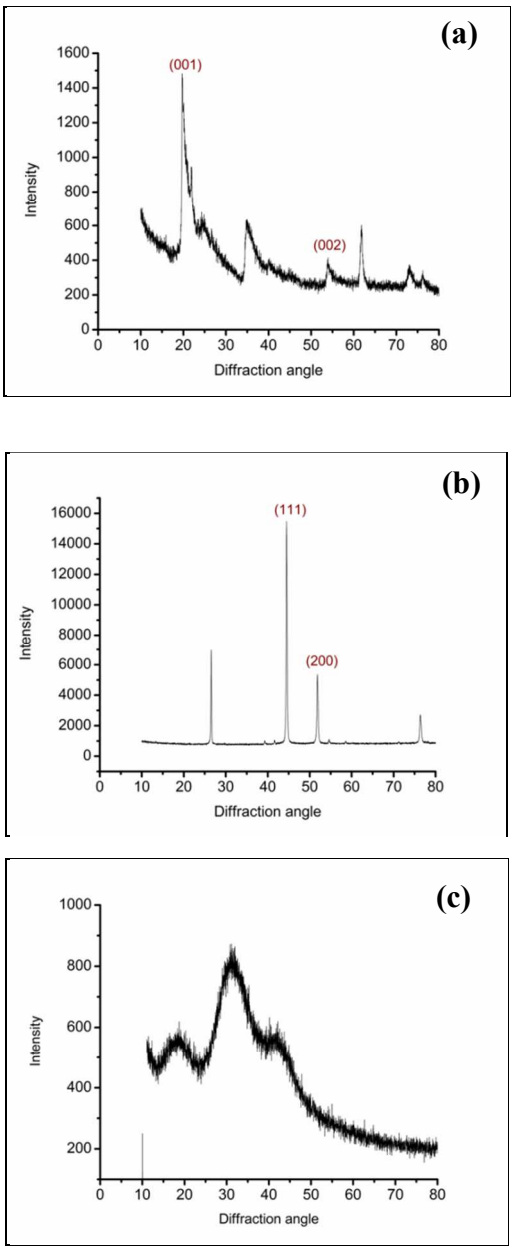

Fig. 5: XRD spectra of (a) unmodified nanoclay (b) Nickel coated nanoclay (c) Hg(II)- nickel coated nanoclay

3.1.4 Roughness

Fig. 6 (a, b) demonstrates the surface morphology of samples with unmodified nanoclay and electroless nickel coated nanoclay investigated using Atomic Force Microscopy. It is evident from the images that the surface roughness of the nanoclay increases by the virtue of electroless nickel coating. The surface roughness for both the surfaces was calculated and is given in Table 1. Nickel coated nanoclay exhibits an increase roughness of almost four times than that of uncoated nanoclay. This nanospike like morphology with uniform pits may be responsible for the increase in the adsorption capacity of nickel coated nanoclay[36]. The formed uniform pits provided high surface area (319.04 nm), which enhances the availability of adsorptive sites for heavy metal ions to get adheres and adsorbed[37].

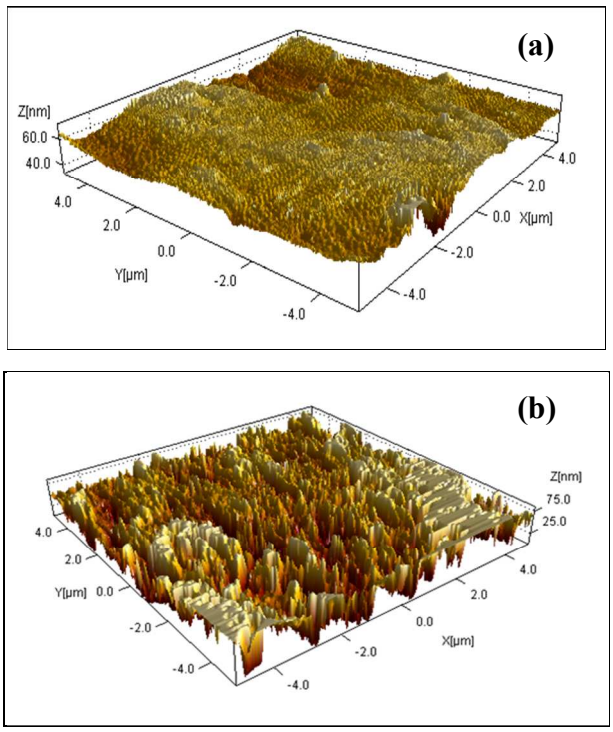

Fig. 6: AFM images of (a) nano-clay (b) Electroless nickel coated nano-clay

Table 1: Average surface roughness of nanoclay and nickel coated nanoclay

Samples	Average Surface roughness (nm)
Unmodified nanoclay	86.78
Nickel coated nanoclay	319.04

3.1.5 Raman Spectroscopy

The Raman spectra of unmodified nanoclay as shown in Figure 7(a) depicts characteristics band at 450, 710 and 1100 cm^{-1} which are mainly contributed to Si-O vibrations. Appearance of peaks at 450 and 710 cm^{-1} represents SiO_4 tetrahedron stretching in the nano-clay. Furthermore, Frost and Rintoul[38] observed that Raman spectra of MMT are difficult to obtain if the layers are dispersed or randomized in their spacing. The representation of other Raman bands for unmodified nano-clay and nickel coated nano-clay are presented in Table 3. Figure 7(b) represents the Raman spectra of nickel coated nano-clay, which assigns the Ni-O stretching vibration at 938cm^{-1}. The emergence of this band represents the coating of nickel over nano-clay surface having various adsorptive sites.

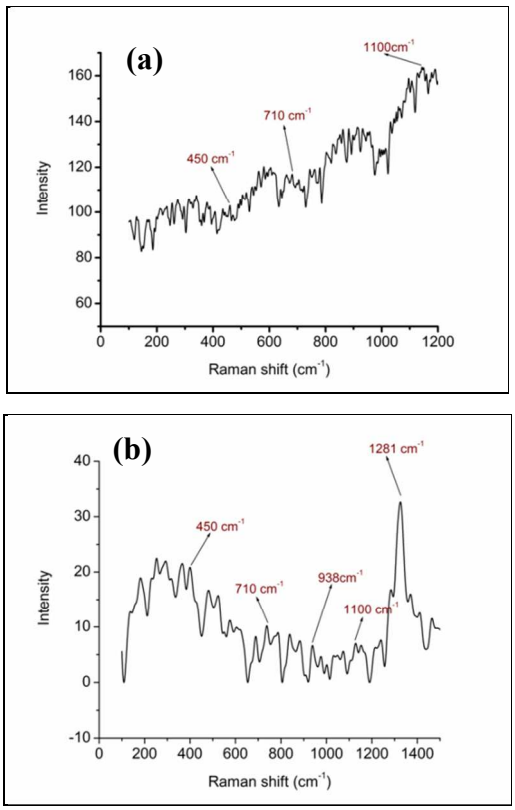

Fig. 7: Raman spectra of (a) unmodified nano-clay (b) Nickel coated nano-clay

Table 2: Raman bands for nanoclay and nickel coated nanoclay

Wavenumber (cm^{-1})	Vibrational modes
450	SiO_4 stretching
710	SiO_4 stretching
1100	C-O and C-C stretching
938	Ni-O stretching
1281	CO-C stretching

3.2 Influence of pH

The variation in adsorption efficiency was monitored with increasing pH from 3.0 to 8.0. The initial pH of the Hg(II) solution was adjusted using dilute HCl or aqueous NaOH solution. According to the stability constant calculations, in highly acidic conditions (pH<4), $HgCl_2$ was the predominant species in the presence of chloride ions. This interrupted the binding of Hg (II) ions onto the sorbent for the reason that, chloride ions tend to form more stable complexes with Hg (II) ions such as $HgCl_2$, $HgCl^-_3$, $HgCl^{2-}_4$ [39]. Besides, at low pH, the excess H^+ ions present in the solution competes with the analyte ions for getting adsorbed onto active sites, resulting in diminished adsorption efficiency [40]. Further, increase in pH, the adsorbent becomes negatively charged and favours uptake of cationic mercury, therefore, retention of 70% was recorded at pH 6.0 which may be ascribed to the ideal number of H^+ ions (Fig. 8). By further increasing the pH, Spontaneous release of nickel was observed due to difficulty in maintenance of exothermicity, hence the mercury starts getting precipitated and lowers the adsorption efficiency[41].

Hence, these results are in good agreement to our previously reported literature[19, 42-44] as shown in Table 3. Hence, pH 6.0 was

picked as an optimum condition for electrolytic removal of Hg (II) ion using the specially designed electrodes.

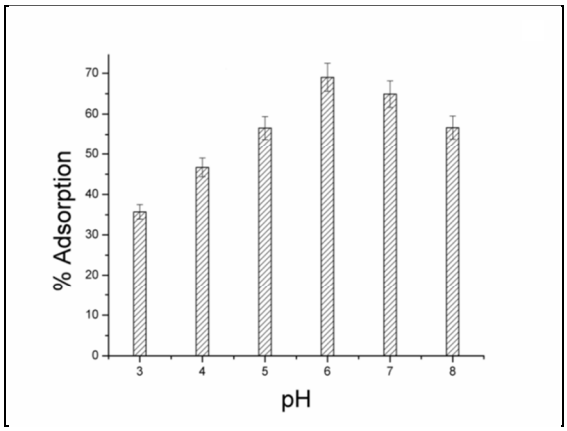

Fig. 8: Variation in % adsorption of Hg(II) with initial pH of the aqueous solution.

Table 3: Removal efficiency of Hg (II) using various adsorbents

Adsorbents	pH	Removal efficiency (%)
Unmodified bamboo leaf powder	8	60.0
Unmodified magnetic iron oxide nanoparticles	8	67.9
Dates nut	10	69.0
Sheep bone charcoal	6	68.4

3.3 Adsorption equilibrium Isotherms

Equilibrium isotherm models are significant to describe the mechanism, process design and efficiency of the adsorption process. It also predicts the distribution of target ions between the liquid and the solid phase. In this study, the equilibrium experimental data for removal of Hg (II) ions was analyzed using the Langmuir and Freundlich models[45]. The isotherm constants were obtained by linear regression method and are presented in Table 4.

3.3.1 Langmuir isotherm model

The Langmuir model assumes monomolecular layer adsorption without any interaction among the adsorbed molecules[46]. The Langmuir model can be represented as:

$$q_e = (q_{max} K_L C_e) / (1+K_L C_e) \quad (3)$$

C_e - equilibrium concentration of metal ions (mg L^{-1}), q_e - amount of metal ions adsorbed (mg g^{-1}), q_{max} - maximum adsorption capacity of the adsorbent for a complete monolayer (mg g^{-1}), K_L - an adsorption constant related to the affinity of the binding sites (L mg^{-1}).

The values of Langmuir constants q_{max} and K_L were obtained by linear regression method. The essential features of a Langmuir isotherm can be expressed in terms of a dimensionless constant, separation factor or equilibrium parameter, R_L which is defined by Hall et al. [47] as:

$$R_L = 1 / (1+K_L C_o) \quad (4)$$

The linear plot (Fig. 9a) yielded the value of R_L as 0.23 (R_L <1 indicates favourable adsorption) and the regression coefficient gives good fit with the experimental data for all systems indicating that equilibrium isotherms can be well described by the Langmuir model.

3.3.2 Freundlich Isotherm model

Freundlich isotherm model considers the occurrence of adsorption process on heterogeneous surfaces. The model relates the maximum adsorption capacity of the adsorbent to the metal ion concentration at equilibrium[48]. This model asserts it applicability to monolayer chemisorption as well as multilayer physisorption processes[49].

The linearized form of equation described by Freundlich model is written as:

$$\ln q_e = (1/n) (\ln C_e) + \ln K_F \quad (5)$$

q_e - equilibrium concentration of metal ions in solid (mg g^{-1}), C_e – equilibrium concentration of analyte ions in liquid phase(mg L^{-1}), n- Freundlich constant related to adsorption intensity and K_F - Freundlich constant associated to adsorption capacity (mg g^{-1}).

The slope and the intercept of the linear plot, ln q_e versus ln C_e (Fig 9b) give the value of 1/n and ln K_F respectively. The value of n obtained from the plot is 8.46 (1/n<10) indicates favourable adsorption) and high value of the regression coefficient (R^2 = 0.99) obtained indicate the applicability of Freundlich model to removal of Hg (II) ions electrolytically. Higher value of n also indicates stronger interactions between Hg (II) ions and the electroless nickel coated nanoclay.

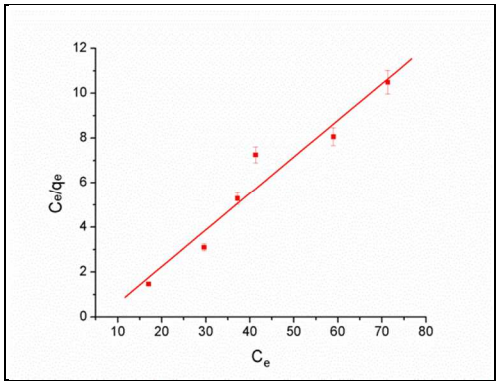

Fig. 9(a): Langmuir equilibrium adsorption isotherm

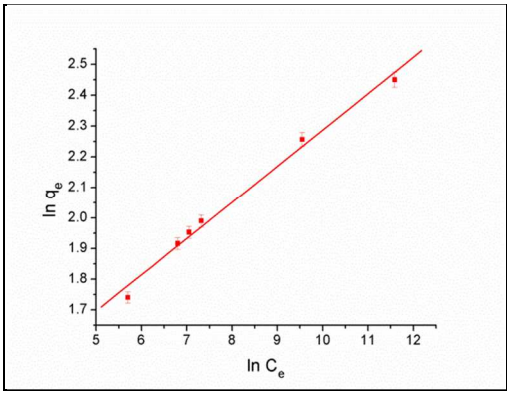

Fig. 9(b): Freundlich equilibrium adsorption isotherm

Table 4: Display of Equilibrium Isotherm Parameters

Isotherm Models	Isotherm Parameters	Values of parameters for Hg(II) ion
Langmuir isotherm Model	q_{max} (mg g^{-1})	6.116
	K_L (L mg^{-1})	0.134
	R_L	0.23
	R^2	0.9405
Freundlich isotherm Model	K_F (mg/g)	3.024
	N	8.47
	R^2	0.99

3.4 Adsorption Kinetics Studies

The knowledge of adsorption mechanism and rate controlling steps holds a pivotal role in selecting optimum conditions for large scale applications[50]. The adsorption mechanism and its potential rate-controlling steps were investigated to analyze the experimental data[51]. Pseudo first-order, pseudo second-order and intraparticle diffusion models have been thoroughly studied to understand the removal mechanism of analyte ions.

3.4.1 Pseudo first-order model

Lagergren and Svenska demonstrated the dependence of rate of adsorption on adsorption capacity of the adsorbent, described by a pseudo first order equation. It is often used to estimate the K_{ad}, considered as mass transfer coefficient in the design calculations. The differential equation is given as[52]:

$$dq/dt = K_1 (q_e - q_t) \quad (6)$$

Integrating Eq. (6) for the boundary conditions t = 0 to t = t and $q_e = q_t$, and rearranging gives:

$$\log (q_e - q_t) = \log q_e - (K_1/2.303)t \quad (7)$$

q_e - amount of Hg(II) ions at equilibrium (mg g^{-1}), q_t - amount of Hg(II) ions at time t (mg g^{-1}), K_1 – first order adsorption rate constant (min^{-1}).

The plot of log (q_e - q_t) versus t yields a straight line (Fig. 10a) and the slope of the line corresponds to first order rate constant (K_1). Table 5 displays the calculated results of the pseudo first-order rate equation. The correlation coefficient values obtained by this method are less than 0.9 suggesting that adsorption mechanism deviates from pseudo first order model.

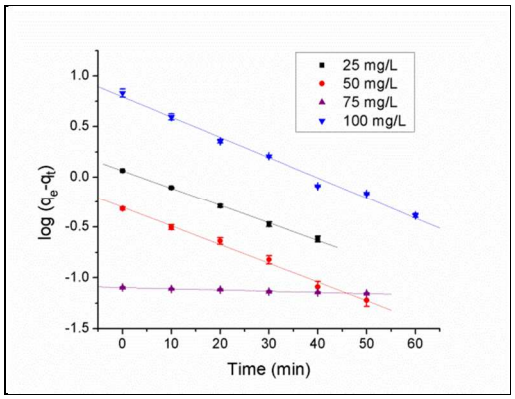

Fig. 10(a): Pseudo first order kinetic model

3.4.2 Pseudo second-order model

According to pseudo second order model described by Ho and McKay, the rate of adsorption is directly proportional to the number of active sites present on the adsorbent surface[53]. The adsorption rate is monitored by the amount of metal ions adsorbed onto the surface of the adsorbent at time t and at equilibrium. The pseudo-second-order differential equation is [52,54]:

$$dq/dt = K_2 (q_e - q_t)^2 \quad (8)$$

Integrating Eq. (8) for the boundary conditions t = 0 to t = t and $q_e = q_t$, and rearranging gives:

$$t/q_t = (1/K_2 q_e) + (t/q_e) \quad (9)$$

q_e - amount of mercury ions at equilibrium (mg g^{-1}), q_t - amount of Hg(II) ions at time t (mg g^{-1}), K_2 - pseudo second-order rate constant (g mg^{-1} min^{-1})

The linear plots of t/q_t vs. t (Fig. 10b) with high correlation coefficient values indicate appropriateness of pseudo second-order model for adsorption of Hg (II) ions.

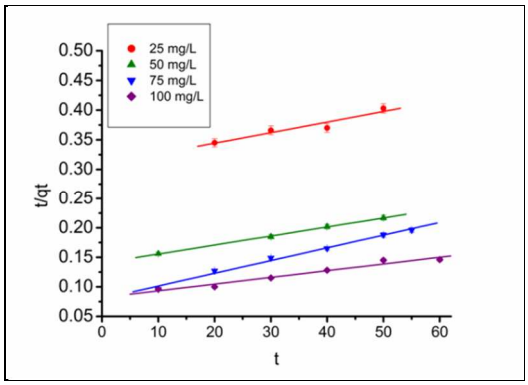

Fig. 10 (b): Pseudo second order kinetic model

3.4.3 Intraparticle diffusion model

According the intraparticle diffusion model proposed by Weber and Morris, the adsorption adsorbate uptake varies proportionally with $t^{1/2}$. The rate-controlling step plays a significant role in determining the removal mechanism and is useful in optimizing conditions for large scale applications. The solid–liquid adsorption process can occur through just by external mass transfer (boundary layer diffusion), intraparticle diffusion (pore diffusion) or conjointly through both. The equation for the model is given as[32]:

$$q_t = K_{int} t^{1/2} + I \quad (10)$$

K_{int} - intraparticle diffusion rate constant (mg $g^{-1}min^{1/2}$), q_t - amount of mercury ions at time t (mg g^{-1}) and I is the intercept.

The plot of q_t versus $t^{1/2}$ passes through the origin and does not exhibit multi-linearity (Fig. 10c), indicating the inapplicability of the model for adsorption of Hg (II) ions onto the nickel coated electrodes[55]. Further, it discards the possibility of diffusion of Hg (II) ions in the middle of electrode bulk.

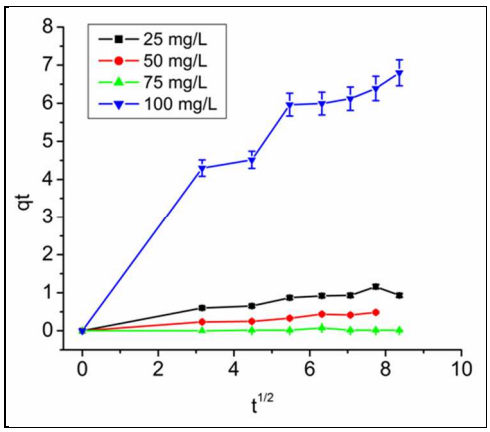

Fig. 10(c): Intra particle diffusion model

Table 5 - Display of Kinetic Parameters

	Conc.	25	50	75	100
Pseudo first-order	K_1 (min^{-1})	0.040	0.043	0.046	0.056
	R^2	0.882	0.889	0.895	0.086
Pseudo second-order	K_2(g/mg min)	0.184	0.329	0.289	0.237
	R^2	0.991	0.989	0.991	0.9912
Intraparticle diffusion	Kint (mg g^{-1} $min^{-0.5}$)	21.12	36.52	54.78	51.45
	R^2	0.930	0.883	0.930	0.9654

4. Conclusions

Electroless nickel coated nano clay was successfully fabricated and employed as the electrode material for electrolytic eradication of Hg (II) ions from mimicked effluent system. SEM and FESEM micrographs depicted the coating of nickel over nanoclay in the form of globules. Electrodes of 10 × 10 × 2 mm dimensions were specially constructed to accomplish the selective elimination of lethal Hg (II) ions. Removal of analyte ions was recorded only after the switch was closed, eliminating the possibility of mercury being adsorbed on the clay surface. Intra particle diffusion model discarded the possibility of diffusion of Hg (II) ions in the middle of electrode bulk. The adsorption followed pseudo-second order kinetics whereas the Freundlich model dominated the equilibrium process indicating multilayer chemical interactions between the adsorbate and the adsorbent. The effectiveness of the proposed method can be further enhanced by optimizing the electrode dimensions and current density. The proposed research provides a fast, feasible, safe and efficient alternative for treatment of contaminated aqueous media containing catastrophic mercury (II) ions in trace and significant amounts.

Acknowledgements

The authors appreciate Defence Institute of Advanced Technology for financial support. Also would like to thanks Dr. Prahlada, Vice Chancellor, DIAT-DU for continuous encouragement and support. We are also grateful to Dr. R.R. Gonte, Prashant rule, Mr HH Kumar (ARDE), Dr. A. Abhyankar, D D Gunjal, Suwarna Raut, Dr. S. Datar, Pramod, Ramdayal Yadav and Yutika Badhe for continuous technical support. The corresponding author would like to dedicate this paper to his Phd Supervisors: Prof. (Dr.) M. Gilbert, Prof. (Dr.) D. Hourston and Dr. G. Wilcox, Department of Materials Engineering, Loughborough University, Leicestershire, UK.

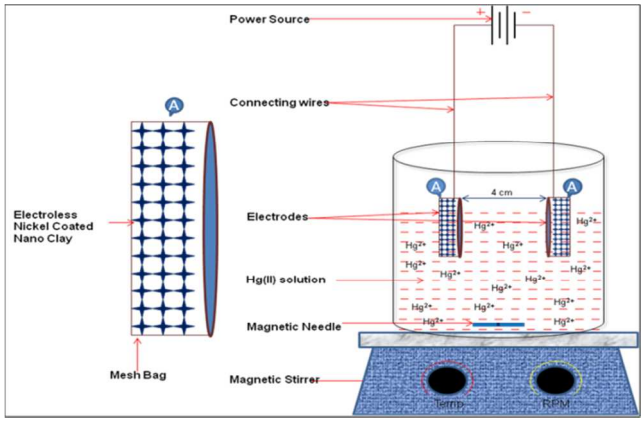

Fig.11: Schematic of the batch experimental setup

Notes and References

[a]*Department of Metallurgical Engineering, Indian Institute of Technology (BHU), Varanasi, India*
[b]*Department of Materials Engineering, Defence Institute of Advanced Technology (DU), Pune, India*
[c]*Department of Applied Physics, Defence Institute of Advanced Technology (DU), Pune, India*
**Email:meetkbs@gmail.com; balask@diat.ac.in*

[1] Dursun, Arzu Y., Biochem. Eng. J., 2006, 28, 187.
[2] D. Park, Y. Yun, J.H. Jo, J.M. Park, Ind. Eng. Chem. Res., 2006, 45, 5059.
[3] E.I. El-Shafey, J. Haz. Mat., 2010, 175, 319.
[4] A.K. Meena, G.K. Mishra, P.K. Rai, C. Rajagopal, P.N. Nagar, J. Haz. Mat. B, 2005, 122, 161.
[5] M. Harada, Crit. Rev. Toxicol., 1995, 25, 1.
[6] Bayramoğlu G, Arica MY., J. Hazard. Mater., 2007,144, 449.
[7] Lai EPC, Wong B, Vandernoot VA., Talanta, 1993, 40, 1097.
[8] E.P.A., National Primary Drinking Water Regulations, 40 CFR Ch.I (7- 1-02 ed.), US Environmental Protection Agency (EPA), Washington, DC, 2002.
[9] X.W.Wu, H.W. Ma, J.H. Li, J. Zhang, Z.H. Li, J. Colloid Interface Sci., 2007, 315, 555.
[10] J.A. Ritter, J.P. Bibler, Water Sci. Technol., 1992, 25, 165.
[11] J. Liu, K.T. Valsaraj, I. Devai, R.D. DeLaune, J. Hazard. Mater., 2008, 157, 432.
[12] R.S. Vieira, M.M. Beppu, Water Res. 2006, 40, 1726.
[13] S. Chiarle, M. Ratto, M. Rovatti, Water Res., 2000, 34, 2971.
[14] C. Miranda, J. Yánez, D. Contreras, R. Garcia, W.F. Jardim, H.D. Mansilla, Appl. Catal. B: Environ., 2009, 90, 115.
[15] M. Velicu, H. Fu, R.P.S. Suri, K. Woods, J. Hazard. Mater., 2007, 148, 599.
[16] X. Ying, Z. Fang, J. Hazard. Mater. B, 2006, 137, 1636.

[17] Li S-X, Zheng F-Y, Yang H, Ni J-C, J. Hazard. Mater., 2011, 186, 423.
[18] Nanseu-Njiki CP, Tchamango SR, Ngom PC, Darchen A, Ngameni E., J. Hazard. Mater., 2009, 168, 1430.
[19] Ayjan Dawlet, Dilnur Talip, Hong Yu Mi, MaLiKeZhaTi, Procedia Environmental Sciences, 2013, 18, 800
[20] Saad SM Hassan, Awaad HA Aboterika, Nasser S Awwad, J. Hazard Mater, 2008, 54, 992.
[21] Wentao H, Yaqin H, Shao chen W, Weikun W, Hao Zh, Carbon, 2011, 49, 838.
[22] RR Gonte , Balasubramanian K, JD Mumbrekar , Journal of Polymers 2013, DOI: 10.1155/2013/309136
[23] A.J.B. Dutra, G.P. Rocha, F.R. Pombo, J. Hazard. Mater., 2008, 152, 648
[23] A.Y.Y. Loo, Y.P. Lay, M.G. Kutty, O.Timpe, M.Behrens, S.B.A.Hamid, Sains Malaysiana, 2012, 41, 213.
[24] M. Spitzer, R. Bertazzoli, Hydrometallurgy, 2004, 74, 3, 233.
[25] Gilbert. M, Kandasubramanian. B , Macromol. Symp., 2005, 221, 185.
[26] A.Y.Y. Loo, Y.P. Lay, M.G. Kutty, O.Timpe, M.Behrens, S.B.A.Hamid, Sains Malaysiana, 2012, 41, 213.
[27] M. A. Barakat, Arabian J. Chem., 2011, 4, 361.
[28] Brunauer S, Emmet PH, Teller E. J Am Chem Soc 1938; 60: 309–319.
[29] Hui Yao, Zhanping You, Liang Li , Shu Wei Goh, Chee Huei Lee, Yoke Khin Yap, Xianming Shi, Construction and Building Materials, 2013, 38, 327.
[30] Herrera, N. N.; Putanux, J. J.; Lami, B. E. Prog. Solid State Chem, 2006, 34, 121.
[31] C. Wan, X. Bao, Feng Zhao, B. Kandasubramanian, M. P. Duggan, Journal of Applied Polymer Science, 2008, 110, 550.
[32] Nitesh Singh, Balasubramanian K., RSC Adv., 2014, 4, 27691.
[33] V. Belova, H. Mhwald, D.G. Shchukin, Langmuir, 2008, 24, 9747.
[34] Feng Zhao, C. Wan, X. Bao, B. Kandasubramanian, Jour. of Colloid and interface, 2009, 333, 164.
[35] C. Wan, Feng Zhao, X. Bao, B. Kandasubramanian, M. P. Duggan, Journal of Physical chemistry, 2008, 112, 11915.
[36] K. Dideriksen, S.L.S Stipp., Geochimica et Cosmochimica Acta, 2003, 67, 3313.
[37] Agnieszka Mierczynska-Vasilev, David A. Beattie, Jou. of Colloid & Interface Sci., 2010, 344, 429.
[38] Frost RL, Rintoul L. Appl Clay Sci 1996; 11: 171–83.
[39] K.A. Krishnan, T.S. Anirudhan, J. Hazard. Mater., 2002, 92, 161.
[40] El-Shafey EI. J Hazard Mater., 2010, 15, 319.
[41] T J Sahetya, F Dixit, Desalination and Waster treatment, 2013, doi: 10.1080/19443994.2013.852483.
[42] Dilip Kumar Mondal, Barun Kumar Nandi, M.K.Purkait, Jou. of Env. Chem. Eng., 2013, doi:10.1016/j.jece.2013.07.034.
[43] H. Parham, B. Zargar, R. Shiralipour, Journal of Hazardous Materials, 2012, 205, 94
[44]Kannan, N Malar, S Jasmin Sugantha, Indian Journal of Chemical technology, 2005, 12, 522.
[45] T.S. Anirudhan, P.S. Suchitra, P.Senan and A.R.Tharun, Ind. Eng. Chem. Res., 2012**,** 51, 4825.
[46] Kumar M, Ando Y, Carbon, 2005, 43, 533.
[47] K.R. Hall, L.C. Eagleton, A. Acrivos, T.Vermeulen, Ind. Eng. Chem. Fundam., 1996**,** 5, 212.
[48] Baudu BM, Derriche Z, Basly JP, J. Hazard.Mater., 2009, 171, 1001.
[49] H.K. Boparai, M. Joseph, D.M. O'Carroll, J. Hazard.Mater., 2011, 186, 1458.
[50] O. Abdelwahab, Egyptian J. Aqua, 2007, 33, 125.
[51] R. Gonte, K. Balasubramanian, Journal of Saudi Chemical Society (2013), doi: http:// dx.doi.org/10.1016/j.jscs.2013.04.003.
[52] H. Qiu, L. LV, B.C. Pan, Q.J. Zhang, W.M. Zhang, Q.X. Zhang, J. SCIENCE A, 2009, 5**,** 716.
[53] Ho, Y.S., McKay G, Process Biochem, 1999, 34, 451.
[54] R.R. Gonte, Balasubramanian. K., J. Hazard. Mater., 2012, 217, 447.
[55] X. Cao, R. Prozorov ,Yu. Koltypin,G. Kataby, I. Felner, A. Gedanken, Journal of mat. Res.,1997, 12, 402.
[56] G. Jiang, M. Gilbert, D. J. Hitt, G. D. Wilcox, K. Balasubramanian, Composites Part A: Applied Science and Manufacturing, 2002, 33, 745.

Figure captions

Fig. 1: Variation of Conductivity of electroless nickel coated nanoclay with volume% nickel

Fig. 2: (a) FESEM image of pristine nano-clay (b) SEM image of nickel coated nano-clay (c) FESEM image of nickel coated nano-clay

Fig. 3: EDX spectrum of electroless nickel coated nanoclay through elemental analysis

Fig. 4: FT-IR spectra of (a) Unmodified Nanoclay (b) Nickel coated nano-clay

Fig. 5: XRD spectra of (a) unmodified nanoclay (b) Nickel coated nanoclay (c) Hg- nickel coated nanoclay

Fig. 6: AFM images of (a) nano-clay (b) Electroless nickel coated nano-clay

Fig. 7: Raman spectra of (a) unmodified nanoclay (b) Nickel coated nanoclay

Fig. 8: Variation in % adsorption of Hg(II) with initial pH of the aqueous solution.

Fig. 9: (a) Langmuir equilibrium adsorption isotherm (b) Freundlich equilibrium adsorption isotherm

Fig. 10: Pseudo first order kinetic model (b) Pseudo second order kinetic model, and (c) Intraparticle diffusion model

Fig. 11: Schematic of the batch experimental setup